Mon. Not. R. Astron. Soc. **373,** 157–166 (2006) doi:10.1111/j.1365-2966.2006.10997.x

The globular cluster kinematics and galaxy dark matter content of NGC 4649 (M60)

Terry Bridges,[1⋆] Karl Gebhardt,[2] Ray Sharples,[3] Favio Raul Faifer,[4,8] Juan C. Forte,[4] Michael A. Beasley,[5] Stephen E. Zepf,[6] Duncan A. Forbes,[7] David A. Hanes[1] and Michael Pierce[7]

[1]*Department of Physics, Engineering Physics & Astronomy, Queen's University, Kingston, ON, Canada K7L 3N6*
[2]*Astronomy Department, University of Texas, Austin, TX 78712, USA*
[3]*Department of Physics, University of Durham, South Road, Durham DH1 3LE*
[4]*CONICET and Facultad de Cs. Astronomicas y Geofisicas, UNLP, Paseo del Bosque 1900, La Plata, Argentina*
[5]*Instituto de Astrofisica de Canarias, La Laguna 38200, Tenerife, Spain*
[6] *Department of Physics and Astronomy, Michigan State University, East Lansing, MI 48824, USA*
[7]*Centre for Astrophysics & Supercomputing, Swinburne University, Hawthorn, VIC 3122, Australia*
[8]*IALP – CONICET, Argentina*

Accepted 2006 August 28. Received 2006 July 16; in original form 2006 February 17

ABSTRACT

From observations with the GMOS multislit spectrograph on the Gemini North telescope, we have obtained spectra for 39 globular cluster (GC) candidates in the Virgo giant elliptical galaxy NGC 4649 (M60), of which 38 are confirmed GCs. The clusters extend out to a radius of 260 arcsec (3.5 effective radii). We find no rotation of the GC system, with an upper limit of $v/\sigma < 0.6$ at a confidence level of 95 per cent. The GC velocity dispersion is constant with radius, within the uncertainties. We fit isotropic models to the GC and stellar kinematics; these models yield an $(M/L)_V$ around 16 at 200 arcsec radius (16 kpc), an increase of a factor of 2 from the central M/L. We also use the mass profile as derived from X-rays to determine the orbital structure. Using axisymmetric orbit-based models and the X-ray mass profile, we find the orbital distribution is close to isotropic within 100 arcsec, and becomes tangentially biased beyond. Furthermore, when using the X-ray profile, we find a better fit to the kinematics compared to using a constant M/L model. Thus, both isotropic and axisymmetric orbit-based models give support for the presence of a dark matter halo in NGC 4649.

Key words: globular clusters: general – galaxies: formation – galaxies: kinematics and dynamics – galaxies: individual: NGC 4649 – galaxies: star clusters.

1 INTRODUCTION

Globular clusters (GCs hereafter) are an excellent way to study the formation, evolution and dark matter (DM) content of galaxies of all types (e.g. Ashman & Zepf 1998; Harris 2001). They are particularly well suited for dynamical studies of early-type galaxies, since they are found in substantial numbers out to large radii around such galaxies and are bright enough to be seen at large distances. GCs complement other dynamical probes such as the stellar light, planetary nebulae (PNe) and X-ray data (e.g. Gerhard 2006; Romanowsky 2006b). Integrated stellar spectroscopy has the advantage of large sample sizes and high signal-to-noise ratio (S/N), which allow the derivation of higher order moments of the velocity distribution, but the faintness of the stellar halo restricts measurement to within a few effective radii of galaxy centres (e.g. Kronawitter et al. 2000; Gerhard et al. 2001). X-ray data can probe further out, and recent high-quality data from *ROSAT*, *ASCA* and *Chandra* have shown that extended dark haloes are a common feature of all luminous ellipticals (Mathews & Brighenti 2003; Humphrey et al. 2006). However, accurate X-ray mass determination requires high-quality gas density and temperature profiles, along with the assumption of hydrostatic equilibrium. As well, only massive ellipticals have hot diffuse gas haloes for mass estimates.

PNe also have extended spatial distributions, and are easily identified because of their strong emission in the [O III] 4959/5007 lines. Romanowsky et al. (2003), using the Planetary Nebula Spectrograph (Douglas et al. 2002), found that three intermediate-luminosity ellipticals (NGC 821, 3379 and 4494) have declining PN velocity dispersion profiles, consistent with simple models with little or no DM. This result is in conflict with the conventional model of galaxy formation, whereby galaxies form in DM haloes. However, numerical

⋆E-mail: tjb@astro.queensu.ca

simulations by Dekel et al. (2005) show that spiral–spiral mergers may lead to halo stars having highly radial orbits, as they are tidally ejected from the inner regions during the merger. Observed PNe in ellipticals, as part of this stellar halo, would then have line-of-sight velocity dispersions lower than that of the underlying DM. Older tracers such as GCs are expected to have higher velocity dispersions, more representative of the DM. In support of this, Sambhus, Gerhard & Mendez (2006) have recently found that the bright and faint PNe in NGC 4697 have different kinematics, and suggest that the bright PNe are a younger population perhaps formed in tidal structures. Our group (Pierce et al. 2006a) has found that the GC velocity dispersion profile in NGC 3379 increases with radius, and non-parametric, isotropic models yield a significant increase in the mass-to-light ratio (M/L) at large radii. A similar result for the NGC 3379 GCs has also been found by Bergond et al. (2006), from FLAMES/VLT data. Note also that Peng, Ford & Freeman (2004a) found a relatively low M/L of 10–15 for NGC 5128 from PNe velocities. It is thus very important to compare GC and PNe kinematics in a larger number of galaxies, to gain a more complete understanding of host galaxy dynamics.

GC velocities have been used to study the dynamics of several early-type galaxies, including M87 (Cohen 2000; Cote et al. 2001), NGC 4472 (Sharples et al. 1998; Zepf et al. 2000; Cote et al. 2003), NGC 1399 (Richtler et al. 2004), NGC 5128 (Peng, Ford & Freeman 2004b) and NGC 3379 (Bergond et al. 2006; Pierce et al. 2006a); see Zepf (2003) for a review. From these studies it is consistently found that the GC velocity dispersions are either constant or increasing with radius. This is strong evidence for DM haloes in these galaxies, supporting X-ray data. Merger simulations (Hernquist & Bolte 1993; Vitvitska et al. 2002; Bekki et al. 2005) predict that ellipticals should have significant amounts of angular momentum at large radius. However, rotation is seen in some GC systems (e.g. NGC 5128; M87), but not in others (e.g. NGC 1399, 3379, 4472). In some cases, the lack of detected rotation may be due to small numbers of GCs; but NGC 4472 and 1399 have hundreds of GC velocities, allowing tight constraints on rotation except at the outer reaches of the data sets. The situation is even more complex when the kinematics of metal-poor (MP) and metal-rich (MR) GCs are studied separately. In most GC systems, the MP and MR GCs are different in terms of their rotation and velocity dispersions, and these differences often depend on galactocentric radius. Usually the MP GCs are dynamically hotter than the MR GCs, as might be expected given their generally shallower spatial profiles (e.g. NGC 5128, 1399, 4472). In some cases (e.g. NGC 4472, M87) the blue and red clusters may be counter-rotating at some radii. In only a few galaxies with the largest GC samples can we say anything about GC orbital anisotropy; in NGC 1399, 4472 and M87 the GCs are consistent with isotropic orbits (though there are hints that the orbital behaviour may be different for MP and MR subsamples).

This paper continues our Gemini/GMOS study of the GC system of NGC 4649 (M60), a bright elliptical located in a subcluster in the eastern part of the Virgo cluster (see Forbes et al. 2004 for further details of NGC 4649 and photometric studies of its GC system). NGC 4649 is well studied in X-rays, with *ROSAT* (di Matteo & Fabian 1997; Trinchieri, Fabbiano & Kim 1997; Bohringer et al. 2000; O'Sullivan, Forbes & Ponman 2001) and *Chandra* (Irwin, Athey & Bregman 2003; Sarazin et al. 2003; Randall, Sarazin & Irwin 2004; Swartz et al. 2004; Gutierrez & Lopez-Corredoira 2005; Humphrey et al. 2006) data. Trinchieri et al. (1997), Bohringer et al. (2000) and Humphrey et al. (2006) all find evidence for an extended DM halo in NGC 4649; Humphrey et al. (2006) find an enclosed mass of 1×10^{12} $M_{\odot}$ and an M/L ~ 5 in the K band at 260 arcsec (20 kpc). *Chandra* data have also revealed over 100 low-mass X-ray binaries (LMXRBs) in NGC 4649 (Sarazin et al. 2003; Randall et al. 2004), and we will use our larger GMOS GC imaging data base (Forbes et al. 2004) to match with the *Chandra* LMXRBs in a future paper (Bridges et al., in preparation).

Previous studies of the stellar kinematics in NGC 4649 have found major axis stellar rotation of 100–120 km s^{-1} out to 45–100 arcsec, a high central velocity dispersion of 350–400 km s^{-1}, and a declining velocity dispersion profile (Fisher, Illingworth & Franx 1995; De Bruyne et al. 2001; Pinkney et al. 2003); de Bruyne et al. also find modest minor axis rotation of $\sim$30 km s^{-1}. de Bruyne et al. use three-integral axisymmetric models to find that a DM halo gives the best fit to the kinematic data, though a constant M/L model is also consistent with the data. We will use the data from Pinkney et al. (2003) to combine with our GC velocities and X-ray data (Humphrey et al. 2006) to study the dynamics of NGC 4649 out to large radius (Section 3.2).

Forbes et al. (2004) presented GMOS photometry for $\sim$1000 GC candidates, and confirmed previous findings of bimodality in the GC colour distribution. Forbes et al. (2004) also found that the red GCs are more concentrated to the galaxy centre than the blue GCs, as is found in many other galaxies. The underlying galaxy light has a similar density profile slope as the red GCs. These GMOS images were used to select GC candidates for follow-up spectroscopy using GMOS in multislit mode (see Section 2.1). This paper presents spectra for 38 confirmed NGC 4649 GCs, and discusses the GC kinematics (rotation and velocity dispersion profiles; Section 3.1) and DM content of NGC 4649 (Section 3.2). In Section 4 we discuss our main results in more detail, while Section 5 presents our conclusions. A companion paper (Pierce et al. 2006b) uses spectroscopic line indices to address the ages, abundances and abundance ratios of the confirmed GCs. We adopt an SBF distance of $D = 17.29^{+0.58}_{-0.56}$ Mpc for NGC 4649 (Mei et al. 2006), taken from the ACS Virgo Cluster Survey (Cote et al. 2004); this gives an image scale of 11.9 arcsec kpc^{-1}. This is slightly larger than the distance of 16.8 Mpc we used in our photometric study of the NGC 4649 GCs (Forbes et al. 2004).

2 MULTI-OBJECT SPECTROSCOPY

2.1 Object selection

GC candidates for follow-up GMOS multislit spectroscopy were selected from our GMOS images taken on 2002 April 10, 11 and 14 (Gemini programme reference number GN-2002A-Q-13). These consist of 4 × 120 s exposures in Sloan g and i filters for three fields. Each field is 5.5 × 5.5 arcmin and the pixel scale is 0.07 arcsec pixel^{-1}; see Forbes et al. (2004) for more details about the pre-imaging. To date, we have only obtained spectroscopy for Field 1, centred 1.9 arcmin to the NE of the galaxy centre (see Fig. 1); the seeing for Field 1 was $\sim$0.6 arcsec. We used the co-added GMOS images provided by Gemini staff for our object selection.

Here is a brief discussion of the procedure we have used to identify a clean sample of GC candidates for spectroscopy. We first median-filtered each image using a square filter $\sim$10 times the image FWHM, and subtracted the medianed image from the original. We then used DAOPHOT to obtain photometry for point-like objects (DAOFIND, PHOT and ALLSTAR). Aperture corrections were then made to obtain total magnitudes. Our photometry was calibrated on to F555W (V) and F814W (I), using *Hubble Space Telescope* (*HST*) WFPC2 photometry kindly provided by Soeren Larsen (Larsen et al. 2001). This calibration was first done on our Field 2, which has the

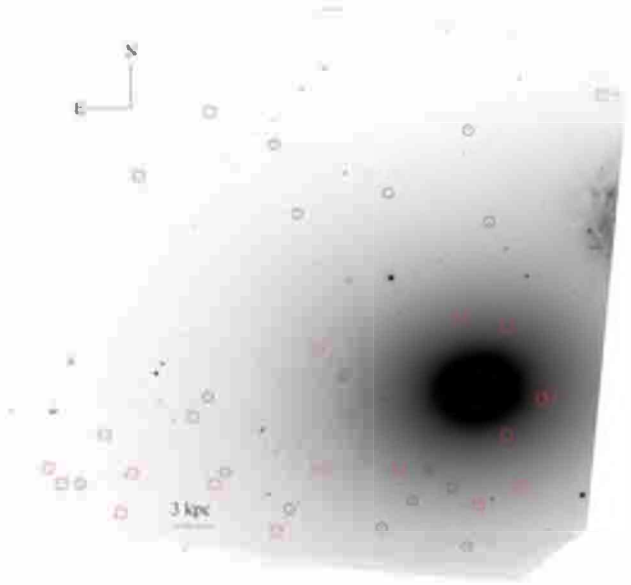

Figure 1. NGC 4649 Field 1. Field orientation is shown at the top left-hand side of the figure. For comparison with Table 1, X (Column 4) increases from bottom to top, while Y (Column 5) increases from left- to right-hand side. NGC 4647 can be seen at the right-hand edge of the frame to the NW of NGC 4649. Confirmed blue GCs are indicated by (blue) circles, and red GCs by (red) squares; the split between blue and red is at $g - i = 1.0$.

most overlap with the *HST* data; we then used overlapping regions between Fields 1 and 2 to calibrate Field 1. We next matched the $g(V)$ and $i(I)$ images. The final result is photometry for ∼800 point-like sources in Field 1, with V, I and $(V - I)$ colours good to ±0.1 mag (sufficient for purposes of object selection).

From this input catalogue, we obtained a final sample of GC candidates by magnitude and colour selection. We selected a magnitude range from $9 < V < 22.5$; the bright cut-off corresponds to where we expect GCs to start appearing at the distance of NGC 4649 (for a distance of 17.3 Mpc, $V = 19$ is $\sim 3.3\sigma$ from the turnover in the GC luminosity function), while the faint cut-off is chosen to give at least a S/N of 5 in an 8-h exposure. Our colour range of $0.75 < V - I < 1.4$ was chosen to include all Galactic GCs (Harris 1996), with some allowance for more MP (bluer) or more MR (redder) GCs. This colour range also encompasses the vast majority of GCs seen in other elliptical galaxies (e.g. Kundu & Whitmore 2001; Larsen et al. 2001). Finally, obviously extended sources were eliminated by eye. After these cuts, 250 objects remained as NGC 4649 GC candidates.

A GMOS multislit mask was made for Field 1 using the standard Gemini GMMPS software. In addition to our GC candidates, we included three stars with $15.5 < V < 18.5$ for mask alignment. Using the B600 grism with a central wavelength of 5000 Å, a slit width of 1 arcsec, and a minimum slit length of 4 arcsec, we were able to allocate 39 slits in Field 1 and the three alignment stars.

2.2 Spectroscopic observations and data reduction

GMOS spectroscopy was obtained for Field 1 on 2003 May 31, June 1, June 4 and June 27, as part of programme GN-2003A-Q-22. A total of 8 × 1800 s exposure was obtained with a central wavelength of 5000 Å, and 8 × 1800 s at 5050 Å; we thus have a total of 8 h on-source time. We used the B600_G5303 grism giving a dispersion of 0.45 Å pixel^{-1} and a resolution of ∼5.5 Å. Spectra typically cover a range from 3300–5900 Å, but the wavelength range depends on the slit position on the mask and some spectra reach up to ∼7000 Å. The seeing ranged from 0.65 to 0.9 arcsec over the four nights. Bias frames, dome flat-fields and copper–argon (CuAr) arcs were also taken for calibration. Typical wavelength residuals of 0.1 Å were achieved.

Data reduction was done in the following way, using the Gemini/GMOS IRAF package (Version 1.6).

(i) GSFLAT was used to make a normalized spectroscopic flat-field from individual flat-field exposures (typically 3 or 4).

(ii) Object frames were bias-subtracted and flat-fielded using GSREDUCE.

(iii) The arc frame was bias-subtracted, but not flat-fielded, using GSREDUCE.

(iv) GSWAVELENGTH was used to establish the wavelength calibration from the CuAr arc frames. This is a 2D fit, and several iterations are required per aperture. This is the most tedious and interactive part of the reduction.

(v) The object frames were then wavelength calibrated using GSTRANSFORM.

(vi) The object frames were then sky-subtracted interactively, using GSSKYSUB.

(vii) GEMCOMBINE was used to create a combined exposure from individual object frames, to act as a reference for extraction of the object spectra (after checking to make sure there are no shifts between the object frames).

(viii) GSEXTRACT was used to extract 1D spectra from each object frame, using the reference frame created in the previous step; optimal (variance) extraction was found to give the best results.

(ix) Finally, SCOMBINE was used to combine spectra from the different object frames; we did a median combine, used AVSIGCLIP for bad pixel rejection, and scaled each individual spectrum by the median of the counts between 4500 and 5000 Å.

The final spectra have S/N ranging from 5 to 21 per Å at 5000 Å, with a median S/N of 11.5 per Å.

2.3 GC velocity determination

To measure the GC velocities, we used the FXCOR task in IRAF. Due to prohibitive time overheads, we did not observe radial velocity standard stars with GMOS. Therefore, we used six Bruzual & Charlot (2003) model spectra for cross-correlation templates. These model spectra have metallicities [Fe/H] of −1.64, −0.33 and +0.1, for ages of 5 and 14 Gyr. We used the average of these six templates for our final velocity (taking a weighted average only changes the velocities by ∼1 km s^{-1}); all cross-correlation peak heights were higher than 0.1 and are therefore very secure. The velocity errors were taken to be the average of the errors returned by FXCOR for the six templates, and thus only reflect the statistical uncertainties in these fits. The final velocities with their errors are given in the last two columns of Table 1.

There was only one background object (a QSO at $z \sim 0.5$) among the 39 spectra. Our low contamination rate of 2.5 per cent is attributable to the good seeing of our GMOS images, and careful colour and magnitude selection. The remaining 38 objects have heliocentric velocities ranging from 484 to 1511 km s^{-1}, and as we discuss in Section 3.1, we believe that these are all GCs belonging to NGC 4649.

Table 1 presents positions, photometry and heliocentric velocities for our 38 confirmed NGC 4649 GCs. Note that the photometry in Table 1 is GMOS Sloan g and $g - i$, taken from Forbes et al.

Table 1. Confirmed GCs around NGC 4649. Cluster ID, RA, Dec., $X, Y, g, g-i$ and heliocentric velocities and errors are presented for 38 confirmed GCs. The g and $g-i$ photometry is from Forbes et al. (2004), while the heliocentric velocities are from this work. To convert to *HST*/WFPC2 V (F555W) and I (F814W) use $V = g - 0.75 \pm 0.1$ and $V - I = g - i - 0.02 \pm 0.1$. The X and Y positions refer to the image shown in Fig. 1; the galaxy centre is approximately at $(X, Y) = (2405, 3664)$. The RA and Dec. have been calculated using ~15 USNO B1.0 stars found in the frame, and the positions are good to ~1 arcsec.

ID	RA (J2000)	Dec. (J2000)	X (pix)	Y (pix)	g (mag)	$g-i$ (mag)	$V_{\rm helio}$ (km s^{-1})	$V_{\rm err}$ (km s^{-1})
89	190.983 978	11.536 740	1324.96	478.67	22.72	1.08	1199.2	43.4
124	190.981 033	11.536 771	1339.40	621.02	21.91	0.88	833.4	59.6
68	190.986 160	11.539 418	1447.41	362.65	22.58	1.22	649.3	33.6
148	190.977 036	11.545 153	1769.64	777.98	22.74	1.14	1184.8	46.8
175	190.974 426	11.531 744	1120.73	961.31	22.29	1.18	852.3	37.6
183	190.972 626	11.538 513	1461.97	1019.24	22.26	1.13	1299.4	35.8
158	190.971 558	11.589 099	3957.80	853.95	23.21	1.16	1261.0	46.0
360	190.949 738	11.594 447	4316.58	1883.79	21.20	0.91	1270.1	40.1
329	190.957 642	11.538 593	1531.35	1741.23	21.93	0.88	1511.2	65.3
277	190.962 753	11.548 118	1978.06	1454.03	22.59	1.04	1299.1	46.5
251	190.960 129	11.599 953	4542.24	1358.58	22.29	1.09	1099.7	43.9
298	190.960 342	11.551 459	2153.17	1556.03	22.58	0.90	1063.0	52.5
318	190.959 274	11.536 565	1424.30	1671.14	23.08	1.00	1173.4	48.6
606	190.936 737	11.548 500	2110.58	2706.89	21.36	1.18	627.0	39.6
558	190.938 461	11.555 140	2430.02	2595.52	21.75	0.74	1087.8	50.8
434	190.949 310	11.528 630	1077.12	2185.82	22.18	1.04	925.9	36.6
462	190.947 189	11.532 343	1269.20	2272.22	22.18	0.92	1112.8	45.4
517	190.942 352	11.539 107	1623.47	2476.30	22.03	1.14	857.2	56.3
412	190.945 847	11.582 625	3751.32	2121.39	22.48	0.95	483.6	47.5
502	190.942 627	11.559 628	2632.89	2375.35	22.10	1.17	688.6	43.5
640	190.931 168	11.586 047	3984.06	2815.36	22.61	0.79	1015.5	104.5
740	190.932 129	11.529 132	1176.86	3012.11	21.68	0.98	962.1	44.8
806	190.929 291	11.538 971	1673.81	3107.00	21.50	1.18	1197.4	46.2
899	190.927 261	11.533 805	1428.31	3227.10	21.44	0.92	1372.0	42.7
975	190.924 591	11.539 021	1696.82	3333.25	20.99	0.92	1052.2	42.3
1063	190.920 807	11.535 969	1563.10	3529.46	21.37	0.94	953.9	47.3
1011	190.918 243	11.596 663	4563.36	3393.26	21.95	0.94	1135.0	45.7
1037	190.919 540	11.564 267	2962.26	3469.39	21.97	1.13	667.9	63.4
1145	190.916 580	11.532 989	1434.77	3745.73	21.60	1.08	1017.1	42.6
1252	190.910 614	11.544 307	2018.25	3985.40	21.27	0.89	926.8	47.3
1384	190.906 281	11.550 952	2364.45	4165.70	20.91	1.03	1134.2	47.0
1126	190.918 457	11.526 026	1083.67	3685.07	22.21	0.90	1122.0	58.2
1298	190.909 515	11.536 103	1619.00	4073.00	22.25	1.13	1346.1	47.9
1211	190.912 033	11.544 750	2033.87	3914.83	22.29	1.01	1324.5	38.0
1098	190.914 841	11.581 110	3812.20	3623.63	22.27	0.77	889.3	69.3
1182	190.911 743	11.562 973	2932.52	3850.43	22.32	1.15	1305.2	39.3
1574	190.896 591	11.602 605	4950.56	4411.99	21.65	1.01	1454.0	45.1
1443	190.904 984	11.551 611	2402.56	4225.51	22.65	1.28	703.0	53.9

(2004); errors in g and $g-i$ are less than 0.05 mag. An approximate conversion to *HST*/WFPC2 V (F555W) and I (F814W) is given by $V = g - 0.75 \pm 0.1$ and $V - I = g - i - 0.02 \pm 0.1$. Fig. 1 shows the spatial distribution of the confirmed GCs.

Two objects deserve separate mention. Object #558 is marginally resolved on our GMOS images, and clearly extended on *HST*/ACS F475W and F850LP images (Proposal 9401: note that the *HST*/ACS images only became public in 2004 July, and we did not have access to them for our spectroscopic object selection). Its velocity (1088 km s^{-1}) is consistent with both that of NGC 4649 (1117 km s^{-1}) or the Virgo cluster (1079 km s^{-1}). Its apparent magnitude is $V = 21.0$, giving it an absolute magnitude $M_V = -10.1$ for a Virgo distance of 16.8 Mpc. It is our bluest object, with $g - i = 0.74$. Thus, its magnitude and colour are consistent with either a luminous GC or a faint (stripped?) dwarf galaxy. Stellar population model fits give an old age and low metallicity for #558, but the fits are uncertain (Pierce et al. 2006b). For the moment, we retain this object in our kinematic sample. Object #1574 is in fact closer in both position and velocity to NGC 4647 than to NGC 4649, and could plausibly be a GC associated with NGC 4647. Exclusion of #1574 changes the mean velocity and velocity dispersions by less than 10 km s^{-1}, and makes no difference to the dynamical modelling in Section 3.2; thus, we retain this object also in our kinematic sample.

3 RESULTS

3.1 Kinematic analysis

3.1.1 Velocity distribution and galaxy membership

Fig. 2 shows both a conventional histogram and a generalized histogram of the velocities for the 38 NGC 4649 GC candidates. The generalized histogram uses an adaptive kernel technique to provide a non-parametric density estimate on a grid; it is explained in detail

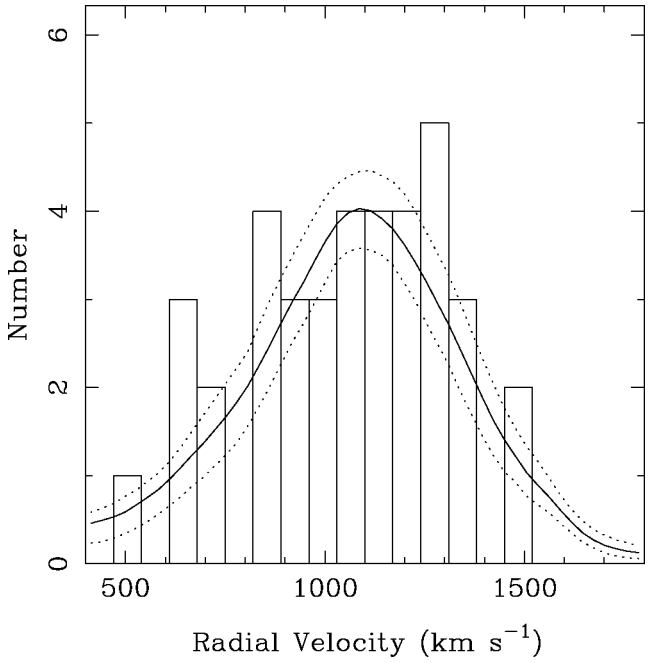

Figure 2. Velocity distribution of NGC 4649 GCs. The bars are a conventional histogram, while the solid and dotted lines are a generalized velocity histogram with 68 per cent confidence intervals.

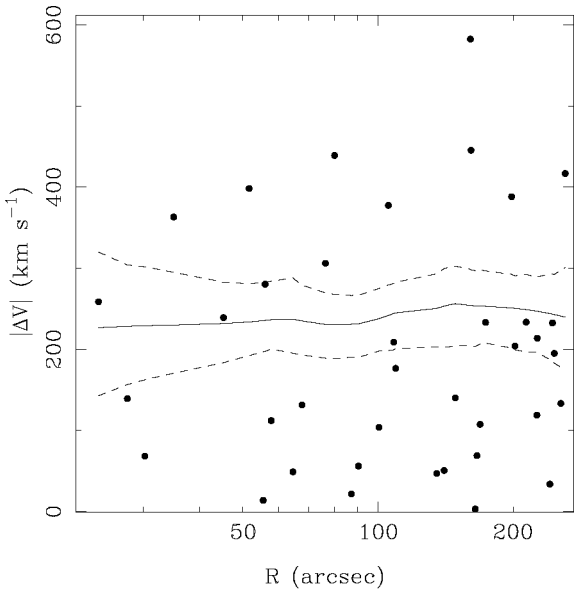

Figure 3. Velocity dispersion versus radius for NGC 4649 GCs. The points are the GC velocities, and the solid curve and dashed lines are the lowess estimator fits with 68 per cent confidence bands.

in Gebhardt et al. (1996). The 68 per cent uncertainties result from Monte Carlo simulations. The systemic velocity of NGC 4649 is 1117 ± 6 km s^{-1} (Trager et al. 2000), the biweight mean velocity for all 38 GC candidates is 1066 ± 45 km s^{-1}, and the median GC candidate velocity is 1094 km s^{-1}.

We first need to determine which of our 38 GC candidates are indeed bona fide NGC 4649 GCs. We first note that the generalized histogram in Fig. 2 shows a very smooth distribution, with no obvious groups of low- or high-velocity non-clusters. Secondly, our lowest candidate velocity is 483 km s^{-1}, and it is very unlikely that a Milky Way field star would have this high a velocity. For instance, 99 per cent of SDSS stars have velocities less than 483 km s^{-1}. We have also ran Besancon models (Robin et al. 2003) for the velocity distribution of halo stars towards NGC 4649 and none had a velocity as high as 483 km s^{-1}. Finally, none of the 41 000+ stars in the Radial Velocity Experiment (RAVE) survey have a velocity as high as 483 km s^{-1} (M. Williams, private communication).

Another approach is to try KMM mixture modelling (McLachlan & Basford 1988; Ashman, Bird & Zepf 1994), to see if there is any evidence for more than one velocity group. We ran the KMM code for two groups, with the first group consisting of the six candidates with velocities 484 $\leqslant V \leqslant$703 km s^{-1} trying both homoscedastic (common covariance) and heteroscedastic groups (independent covariance). We also tried running KMM with the first group consisting solely of the lowest velocity candidate at 483 km s^{-1}, but the result was identical to the first case. In no case did we find that two groups were a statistically better fit to the velocity distribution than one (P-values of 0.25 and 0.52 for homoscedastic and heteroscedastic groups, respectively).

We conclude that all of the 38 GC candidates are indeed bona fide GCs belonging to NGC 4649 (but note that there is uncertainty about whether object #1574 belongs to NGC 4649 or 4647, as discussed in Section 2.3).

3.1.2 Velocity dispersion

We have used the ROSTAT code (Beers, Flynn & Gebhardt 1990) to calculate the biweight velocity dispersion for the NGC 4649 GCs. We have done this for all of the GCs, and for the blue and red GCs separately. The division between blue and red GCs is at $(g - i) = 1.0$, based on the bimodality in the GC colour distribution seen in Forbes et al. (2004). The velocity dispersion for all 38 GCs (256 ± 29 km s^{-1}) is comparable to the dispersions found in other early-type galaxies. The velocity dispersion for the red GCs (288 ± 43 km s^{-1}) is higher than for the blue GCs (205 ± 65 km s^{-1}), in contrast to other luminous ellipticals. To see how sensitive these results are to our colour boundary, we have set the boundary at $(g - i) = 0.95$ and $(g - i) = 1.05$; the blue/red dispersions are 181 ± 50/297 ± 39, and 222 ± 44/286 ± 53, for a boundary of $(g - i) = 0.95/1.05$. The dispersions, especially for the blue GCs, are sensitive to the adopted colour boundary, but the difference in dispersion between the red and blue GCs persists for all three choices. The red GCs thus have a higher velocity dispersion than the blue GCs of 64–116 km s^{-1}, but at a low significance level ranging from 0.9 to 1.8σ.

Fig. 3 shows the GC velocity dispersion radial profile. This dispersion profile was derived using the lowess estimator, which runs a radial window function through the data to estimate the velocity squared (see Gebhardt & Fischer 1995, and Pierce et al. 2006a for further details). Fig. 3 shows that the GC velocity dispersion profile is constant with radius within the errors. We have checked whether removal of the young and intermediate age clusters, as discussed in Pierce et al. (2006b), changes the dispersion values; within the uncertainties there is no change in the results.

3.1.3 Rotation of the globular cluster system

We have searched for rotation in the GC system by doing non-linear least-squares fits to the following equation:

$$V(\theta) = V_{\rm rot} \sin(\theta - \theta_0) + V_0,$$

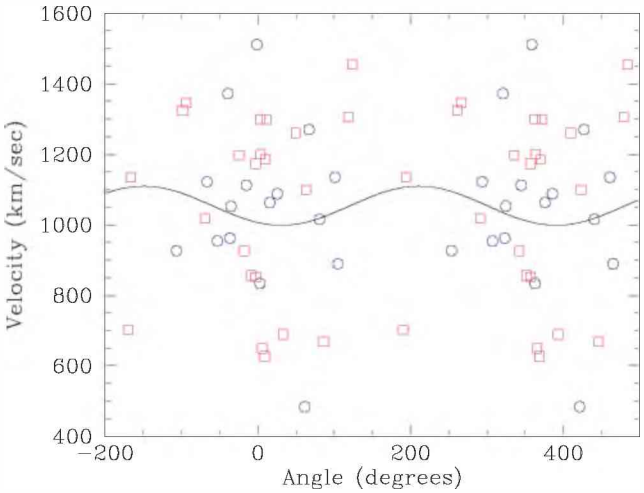

Figure 4. Velocity versus azimuthal angle for all (38) NGC 4649 GCs. Blue GCs are the open circles, and the red GCs are the open squares. The solid line is the best-fitting rotation curve for all GCs, returned by the fitting code. No significant rotation is seen in any NGC 4649 GC sample.

where $V_{\rm rot}$ is the GC rotation velocity (amplitude), θ is the GC azimuthal angle, θ_0 is the position angle of the line of nodes, and V_0 is the systemic velocity of NGC 4649. This determines the best-fitting flat rotation curve; see Zepf et al. (2000) for more details.

We have fit the above equation for all three GC samples (total, blue and red). Because of the small numbers of GCs, we fixed V_0 at the mean GC velocity (1066 km s^{-1}). The GC mean velocity and systemic velocity of NGC 4649 differ by about 50 km s^{-1}. Since we are measuring rotation and because our GC sample is not centred on the galaxy, by using the GC mean rotation, we may be removing rotation at the level of 50 km s^{-1}. Thus, we will likely be underestimating the true rotation. We have also looked for rotation using the systemic velocity, but find small differences. In either case, rotation is not significant. Fig. 4 shows the GC velocities as a function of azimuthal angle, with the 'best-fitting' rotation curve for all GCs superimposed. It is clear that the data in Fig. 4 show no rotation signature. This is confirmed by our quantitative fitting, which yields a rotation of 57 ± 58 km s^{-1} for all GCs, and similar null results for blue and red GCs considered separately. In summary, there is no significant rotation in any of the GC samples.

We have used Monte Carlo simulations to set an upper limit on the rotation velocity for all GCs. We generate artificial samples with the same position angle distributions and velocity dispersions as the data, but with a rotation curve of given amplitude imposed. The 95 per cent confidence upper limit is defined as the rotation velocity for which only 5 per cent of these simulations give a rotation velocity as small as that observed (see Zepf et al. 2000). We find a 95 per cent upper limit of 150 km s^{-1} for the rotation amplitude of all GCs. Combined with the velocity dispersion of 256 km s^{-1} (Section 3.1.2), we derive an upper limit for the ratio of rotation amplitude to velocity dispersion of $v/\sigma < 0.6$.

It is of course possible that rotation is present in the NGC 4649 GC system, but we have failed to detect it. The main factor is our poor spatial and azimuthal coverage (see Fig. 4 for our uneven azimuthal coverage). As well, while our total sample of 38 GCs is reasonable, the blue and red GC sample sizes are smaller than we would like. We plan to acquire more velocities in our other two fields, which will alleviate the above difficulties and allow us to set tighter constraints on the presence or absence of rotation.

3.2 Dynamical models

We use two approaches to measure the M/L profile in NGC 4649. As a first step, we use spherical, isotropic models applied to the stellar kinematics and the GC kinematics. With only 38 GC velocities, it is hard to go much beyond the isotropic assumption without additional constraints. While we fully understand the limitations with these assumptions, we argue that for comparative value, isotropic models are informative since many previous studies have relied on these. Our second approach uses fully general axisymmetric models. These models are based on Schwarzschild (1979), where one runs a set of orbits in a specified potential and fits for the orbital weights to best match the observational constraints. However, since these models are so general (i.e. allowing anisotropy as a free parameter spatially in both radius and angle), 38 velocities will be inadequate to overcome the uncertainties in both the potential and orbital structure. Fortunately, NGC 4649 has a detailed mass model from *Chandra* X-ray observations (Humphrey et al. 2006). Thus, we use the M/L profile as determined from X-rays as the input into the orbit-based models, which then provide the best-fitting orbital structure. Both techniques give the same answer, that NGC 4649 requires a substantial increase in the M/L at large radii.

3.2.1 Isotropic models

The isotropic models are straightforward and follow the approach outlined in Pierce et al. (2006a). Briefly, we use non-parametric models assuming isotropy (see Gebhardt & Fischer 1995). We use both the GC velocities and stellar kinematic data for the inner 70 arcsec from Pinkney et al. (2003). For the surface brightness profile, we use the stellar light profiles of Lauer et al. (2005) and Caon, Capaccioli & Rampazzo (1990), where the latter extends out to over 700 arcsec. The Lauer et al. (2005) profile is in the V band, and we transform the Caon et al. (1990) B-band profile by matching in the overlap region. We find $B-V=0.98$. We apply an extinction correction of $A_V = 0.088$ (Schlegel, Finkbeiner & Davis 1998). However, since we are fitting the GCs, we should in fact be using their number density profile. Forbes et al. (2004) compare the GC profile to the stellar profile. They find that the red GCs are very similar to the stellar profile, whereas the blue GCs are slightly flatter. Given the uncertainties in these profiles, and that there are more velocities from the red GCs, use of the stellar light profile is reasonable.

Fig. 5 shows the results. The upper panel shows the combined stellar and GC velocity dispersion [solid (red) line], with 1σ errors (red hatched region). The dashed (black) curve in the upper panel is the expected isotropic velocity dispersion profile for a constant M/L (i.e. no DM). The GC data are inconsistent with the constant M/L model over most of the radial range. The lower panel shows the projected $(M/L)_V$ ratio for the stellar and GC data with 1σ errors [solid (red) line and hatched region], and the dashed (blue) line is the *Chandra* X-ray $(M/L)_V$ profile from Humphrey et al. (2006). The X-ray analysis of Humphrey et al. (2006) provides the total mass, and we convert to M/L by dividing by our V-band light profile. The GC data show an increasing M/L with radius, in other words implying a DM halo in NGC 4649. There is excellent agreement between the GC and X-ray mass profiles, reinforcing the evidence for this DM halo.

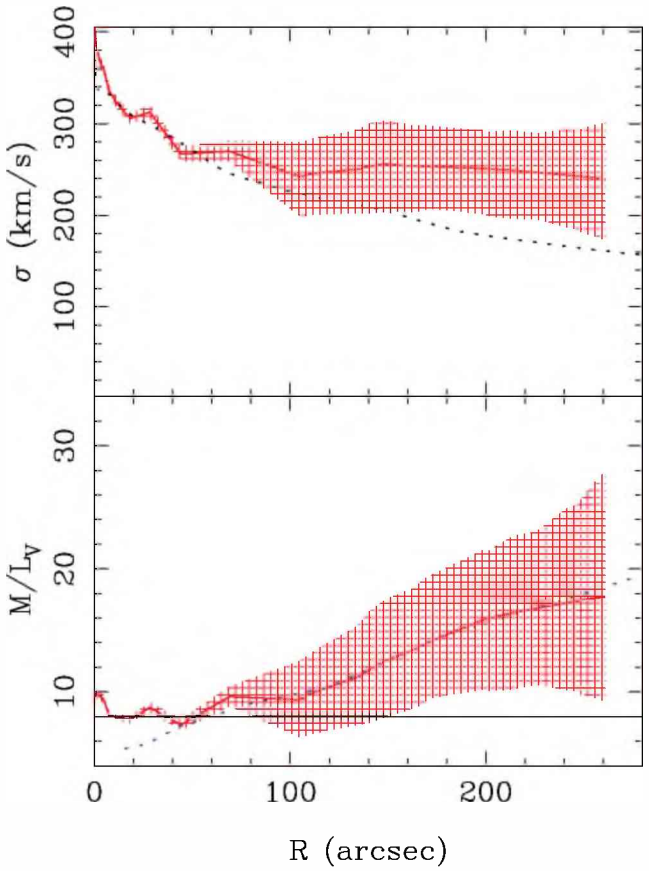

Figure 5. Upper panel: velocity dispersion against projected radius for NGC 4649 GCs and stellar data. The solid (red) line is the GC data, with 1σ errors (red hatched region). The dashed (black) line is the expected isotropic dispersion profile for a constant M/L model. Lower panel: $(M/L)_V$ as a function of projected radius for the NGC 4649 stars, GCs and X-ray emission. The solid (red) line is the profile for the stars and GCs, and the red hatched region are the 1σ errors. The dashed (blue) line is the profile for the X-ray emission, obtained from the X-ray mass profile of Humphrey et al. (2006) and our V-band light profile. The horizontal line with $(M/L)_V = 8$ represents the value adopted for the constant M/L model in Section 3.2.2. For our assumed distance of 17.3 Mpc, 100 arcsec corresponds to a linear radius of 8.1 kpc. The effective radius R_e for NGC 4649 varies between 42 arcsec in the K band (Jarrett et al. 2003) and ~80 arcsec in the optical (Faber et al. 1989; van der Marel 1991).

3.2.2 Orbit-based models

All aspects of the axisymmetric orbit-based models are provided in four papers: Gebhardt et al. (2000, 2003) and Thomas et al. (2004, 2005). Thomas et al. (2005) provides the most direct comparison since it studies dark halo properties. Briefly, we first input a potential, either from stellar light only or a known mass profile (i.e. the X-ray potential). We then run a set of orbits in that potential that covers the available phase space. Thomas et al. (2004) provide a detailed description of the orbit sampling. For NGC 4649, we use approximately 10^4 orbits and 255 observational constraints. We then determine the non-negative orbital weights that best match the observational constraints. We use entropy as a way to facilitate the χ^2 minimization over this large set of parameters. The use of entropy as a way to regularize the models has very little effect on the results (as we discuss below).

For the potential, we use both the stellar light profile and the X-ray profile. The stellar light profile is the same as used above for the isotropic models, except we now include the proper axis ratio of 0.88. We assume that the galaxy is edge-on. We run two sets of orbits: one for a constant stellar M/L [taking $(M/L)_V = 8$; see Fig. 5], and one with a profile that uses a constant stellar M/L [again $(M/L)_V = 8$] out to 45 arcsec and following the X-ray M/L profile beyond that. At the outer limit of the model, the increase in the M/L is a factor of 2.5 from the central regions (inside 45 arcsec). For completeness, we include a central black hole as reported in Gebhardt et al. (2003); this will likely effect the kinematics near the centre only, but since we desire the orbital structure throughout the galaxy, it is important to include as realistic a potential as possible. The model is the same as in Gebhardt et al. (2003), where we divide the model in spatial bins consisting of 20 radial and five angular bins. The orbit sampling as outlined in Thomas et al. (2005) allows for very efficient coverage of the available phase space of the distribution function.

The kinematics come from published results in Pinkney et al. (2003) and the GC velocities presented here. Pinkney et al. (2003) have fairly extensive stellar kinematics along three position angles and go out to 70 arcsec along the major axis. For the GCs, we only use those beyond the stellar data, and we only use them in three radial bins. We measure the velocity dispersions from the GCs using a maximum-likelihood approach that includes the uncertainties directly (as discussed in Pryor & Meylan 1993). The three dispersion values give approximately the same results as the lowess estimator. The three radial bins are at $R = 118, 183, 240$ arcsec with dispersion values of 230 ± 60, 270 ± 75, 220 ± 70 km s^{-1}, respectively. Since the GCs are spread over the full angular range of the galaxy, we sum up the model angular bins in the same way (as opposed to the stellar kinematics, which are along particular position angles).

There are two main ways in which to use the orbit-based models. First, one can use the fit in a χ^2 sense to determine which potential gives the best fit to the data. In this way, one would run orbits in a large set of potentials and then choose which one has the lowest χ^2 as the best model. The second result from the orbit models is that for a given potential, the model produces a distribution function that optimizes the fit to the observations. Thomas et al. (2004, 2005), as well as Cappellari et al. (2006), have done many tests determining the ability to recover the distribution function using analytic models. If one has adequate radial and angular coverage, then the distribution function can be recovered robustly. In the case of NGC 4649, we are unlikely to get detailed information on the distribution function, but should be able to obtain reliable projections of it. For example, as shown in Gebhardt et al. (2003) and Gebhardt (2004), the simple ratio of the radial to tangential dispersions as a function of radius and angle is a useful and robust quantity. Thus, for NGC 4649 we concentrate on this ratio. The program obviously provides both angular dispersions: the azimuthal (parallel to the equatorial plane) and the polar (perpendicular to the equatorial plane). We add in quadrature the two angular dispersions and average, and compare this quantity to the radial dispersion. Thus, isotropic models have radial and tangential dispersions equal to each other.

Fig. 6 shows the internal dispersion ratio for the potentials using the M/L profile from X-rays (upper panel) and a constant M/L (lower panel), along each position angle. For the X-ray profile, the orbital structure becomes slightly tangentially biased beyond 100 arcsec; the average ratio is about 0.8. For the constant M/L model, the average ratio is about 0.7. The stronger tangential bias in the constant M/L model is what one would expect if a dark halo is present but not included in the dynamical models. One way to increase the projected dispersions at large radii is to put more energy into the tangential component.

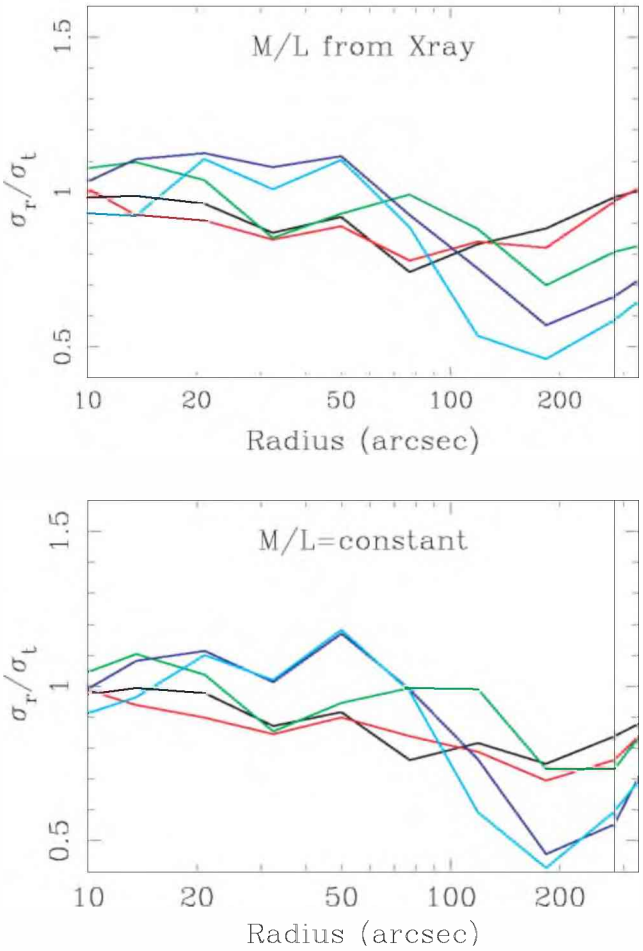

Figure 6. The ratio of the radial to the tangential velocity dispersion along the five position angles in the orbit-based models. A ratio of 1 would imply an isotropic model. The vertical solid line is the radial extent of the observations; results beyond that radius are not meaningful. The top panel assumes a mass profile as determined from the X-ray observations of Humphrey et al. (2006), and the bottom panel assumes a mass profile from the stellar light with a constant M/L. Using the mass profile from the X-rays produces less tangential bias at large radii, although some is still present implying either a need for a larger M/L increase or a real effect in the GC orbits.

Due to the large uncertainties in the kinematics from the GCs, we have not explored other dark halo models beyond the X-ray potential. However, we note that the overall fit to the data is better with the X-ray potential than with the constant M/L model. The change in χ^2 is 5, implying a significance of greater than 95 per cent. Thus, with these data and the X-ray potential alone, we find a strong significance for a dark halo. A further test would be to try a variety of dark halo models. Since we only tried one, it is very likely that the minimum χ^2 will be even lower, implying a yet higher significance. Thus, we have not determined the best-fitting dark halo model for this data set; this implies that we have not found the best-fitting orbital structure as well. Presumably, if the dark halo were more massive than the X-ray model suggests, we would find an orbital structure that is more consistent with isotropy. However, this test does demonstrate the power of combining X-ray data and kinematics. If we take the X-ray potential as truth, then the underlying orbital distribution is as given in Fig. 6; that is, the GCs are nearly isotropic out to 100 arcsec, and tangentially biased beyond that radius.

4 DISCUSSION

We have not detected any rotation in the NGC 4649 GC system, with $v/\sigma < 0.6$ for all GCs. As discussed in Section 1, there is considerable variation in the rotation properties of GC systems amongst early-type galaxies. Projection effects certainly play some role in explaining this variation, but these effects have not been properly studied to date. A range of rotation properties is also seen from PN data, with several ellipticals showing little rotation ($v/\sigma \sim 0.2$; Romanowsky 2006a). Yet most simulations of elliptical galaxy formation predict significant amounts of angular momentum in their outer haloes (e.g. Barnes 1992; Vitvitska et al. 2002). One possibility is that angular momentum is transported beyond the radial range of our data, which is ~20 kpc or 3.2–6.5 R_e. Simulations also show that the angular momentum of DM haloes is generally larger for major mergers, and lower for multiple accretion of satellites (Gerhard 2005). Thus, the merging history of ellipticals may also play a role in determining their rotation. It is interesting to note in this context that there is no evidence for a major merger (or indeed any recent interaction) in NGC 4649. Pierce et al. (2006b) have found several young (2–3 Gyr) GCs in NGC 4649. The origin of these young GCs is not clear, but the fact that GCs younger and older than 9 Gyr have very similar velocity dispersions (see Section 3.1.2) argues against the young GCs having been formed in a merger.

We have also been able to put constraints on the orbital structure of the GCs, through the use of orbit-based models with a specified potential. We find that the GC orbits are close to isotropic out to 100 arcsec, but become tangentially biased at larger radii (Fig. 6). Unfortunately, there are very few early-type galaxies with which we can compare our results. An analysis similar to ours for NGC 4649 has been carried out for M87 (Cote et al. 2001) and M49 (Cote et al. 2003). In both galaxies, the entire GC system is close to isotropic at all radii. There are differences, however, when the MP and MR GCs are considered separately. In M87, the MP GCs are tangentially biased at all radii, particularly within 15 kpc, while the MR GCs are isotropic or slightly tangentially biased within 15 kpc, and radially biased beyond this radius. In M49, the MP GCs are close to isotropic, while the MR GCs become tangentially biased at large radius. Richtler et al. (2004) were able to place weak constraints on the orbital structure of the NGC 1399 GCs, finding that the MR GCs are close to isotropic, and that the MP GCs have a slight tangential bias. Overall then, existing data show that GCs in early-type galaxies generally have orbits that are close to isotropic, but there may be differences in the orbital structure of MP and MR GC subsystems. Unfortunately, our small sample size does not allow us to investigate such possible differences in the MP and MR GCs in NGC 4649. The models presented in this paper use axiysmmetric orbit-based models, which are the most general models one can run assuming axisymmetry, and thus should provide the fairest description of the orbital structure. The previous models listed above are all based on spherical symmetry, and it may be that once more realistic models are used, a clear picture of the outer structure may emerge.

We have found evidence for a DM halo in NGC 4649 from both spherical, isotropic models and axisymmetric, orbit-based models. The isotropic models give an $(M/L)_V$ of 9–28 at 260 arcsec radius (~21 kpc; Fig. 5). The isotropic GC M/L profile (Fig. 5) gives excellent agreement with the *Chandra* M/L profile (Humphrey et al. 2006). De Bruyne et al. (2001) also found evidence for a DM halo

from their stellar kinematic data extending to ∼90 arcsec. Fig. 5 shows that the NGC 4649 M/L is ∼8 near the galaxy centre, and starts increasing at ∼50 arcsec. There is a significant difference between the effective radius R_e for NGC 4649 in the optical and infrared, with optical values between 70 and 80 arcsec (de Vaucouleurs et al. 1991; Faber et al. 1989; van der Marel 1991), and a 2MASS K-band value of 42 arcsec (Jarrett et al. 2003). In any case, both X-ray and GC data suggest that NGC 4649 is becoming DM dominated beyond ∼1 R_e, as has been found for other ellipticals (Mamon & Lokas 2005; Gerhard 2006; Romanowsky 2006b).

DM haloes are commonly found in other early-type galaxies from GC, X-ray and stellar kinematic data (see Section 1; Gerhard 2006; Napolitano et al. 2005). However, PN data have been used to argue against the existence of DM haloes in early-type galaxies (e.g. Romanowsky et al. 2003). As discussed in Section 1, this may be because PNe in early-type galaxies are on preferentially radial orbits. For cluster galaxies there is the added complication of potential contamination from intracluster PNe (e.g. Feldmeier et al. 2004). Unfortunately, there are no published PNe data for NGC 4649 to compare our GC results with. GC spectroscopy allows both the determination of velocities and ages/abundances, allowing us to investigate whether kinematics depends on age. However, even with 8-m class telescopes, it is difficult to obtain the high-S/N spectra needed for reliable age determination, so there is little age data available at present. We have found that exclusion of four young (2–3 Gyr: #89, 175, 502, 1443) and two intermediate-age (5–6 Gyr: #517, 1182) GCs in NGC 4649 (see Pierce et al. 2006b) has no significant effect on the M/L profile, but our GC sample size is not large. More kinematic data for a range of tracers, including PNe, GC, stellar and X-ray, are needed for NGC 4649 and other early-type galaxies.

5 CONCLUSIONS

We have used Gemini/GMOS to obtain spectra for 38 confirmed GCs in NGC 4649. The recession velocities of these clusters have been used to study the cluster kinematics and DM content of NGC 4649. Our main results are as follows.

(i) The GC velocity dispersion profile is constant with radius, for all GCs, and also for the blue and red GCs separately.

(ii) We detect no rotation in the GC system, both for all clusters, and for blue and red samples separately. We are able to place upper limits on the ratio of rotation velocity to velocity dispersion $v/\sigma < 0.6$ for all GCs. Further data to improve our spatial and azimuthal coverage, and our sample size, are needed to make further progress.

(iii) Both spherical, isotropic and axisymmetric, orbit-based dynamical models strongly support the presence of a DM halo in NGC 4649. For the isotropic models there is excellent agreement between the stellar plus GC M/L profile and the X-ray M/L profile from Humphrey et al. (2006).

(iv) Within ∼100 arcsec radius, the GC orbits are close to isotropic, while at larger radius the orbits become tangentially biased.

ACKNOWLEDGMENTS

We thank the anonymous referee for a thorough reading of this paper, and for several useful suggestions which have significantly improved the paper. We would like to thank Inger Jorgensen and Gemini staff astronomers for wonderful support for our GMOS programme. We are very grateful to Soeren Larsen for sharing his *HST* data with us. DAF thanks the ARC for its financial support. SEZ acknowledges support for this work in part from the NSF grant AST-0406891 and from the Michigan State University Foundation. This research was supported in part by a Discovery Grant awarded to DAH by the Natural Sciences and Engineering Research Council of Canada (NSERC). KG acknowledges support from NSF CAREER grant AST-0349095. JCF and FRF have been supported with grants from CONICET and Agencia Nac. de Promocion Cientifica, Argentina. These data were based on observations obtained at the Gemini Observatory, which is operated by the Association of Universities for Research in Astronomy, Inc., under a cooperative agreement with the NSF on behalf of the Gemini partnership: the National Science Foundation (USA), the Particle Physics and Astronomy Research Council (UK), the National Research Council (Canada), CONICYT (Chile), the Australian Research Council (Australia), CNPq (Brazil) and CONICET (Argentina). The Gemini programme ID is GN-2002A-Q13. This research has made use of the NASA/IPAC Extragalactic Database, which is operated by the Jet Propulsion Laboratory, Caltech, under contract with the National Aeronautics and Space Administration.

REFERENCES

Ashman K. M., Zepf S. E., 1998, Globular Cluster Systems. Cambridge Univ. Press, Cambridge
Ashman K. M., Bird C. M., Zepf S. E., 1994, AJ, 108, 2348
Barnes J. E., 1992, ApJ, 393, 484
Beers T. C., Flynn K., Gebhardt K., 1990, AJ, 100, 32
Bekki K., Beasley M., Brodie J. P., Forbes D. A., 2005, MNRAS, 363, 1211
Bergond G., Zepf S. E., Romanowsky A., Sharples R. M., Rhode K. L., 2006, A&A, 448, 155
Bohringer H. et al., 2000, ApJS, 129, 435
Bruzual G., Charlot S., 2003, MNRAS, 344, 1000
Caon N., Capaccioli M., Rampazzo R., 1990, A&AS, 86, 429
Cappellari M. et al., 2006, MNRAS, 366, 1126
Cohen J. G., 2000, AJ, 119, 162
Cote P. et al., 2001, ApJ, 559, 828
Cote P., McLaughlin D. E., Cohen J. G., Blakeslee J. P., 2003, ApJ, 591, 850
Cote P. et al., 2004, ApJS, 153, 223
De Bruyne V., Dejonghe H., Pizella A., Bernardi M., Zeilinger W. W., 2001, ApJ, 546, 903
De Vaucouleurs Y., de Vaucouleurs A., Corwin H. Y., Jr, Buta R. J., Paturel Y., Fouqué P., 1991, Third Reference Catalog of Bright Galaxies. Springer Verlag, New York
Dekel A., Birnboim Y., 2006, MNRAS, 368, 2
Dekel A., Stoehr F., Mamon G. A., Cox T. J., Novak G. S., Primack J. R., 2005, Nat, 437, 707
di Matteo T., Fabian A. C., 1997, MNRAS, 286, 50
Douglas N. et al., 2002, PASP, 114, 1234
Faber S. M., Wegner G., Burstein D., Davies R. L., Dressler A., Lynden-Bell D., Terlevich R. J., 1989, ApJS, 69, 763
Feldmeier J. J., Ciardullo R., Jacoby G. H., Durrell P. R., 2004, ApJ, 615, 196
Fisher D., Illingworth G., Franx M., 1995, ApJ, 438, 539
Forbes D. A., 2005, ApJ, 635, L137
Forbes D. A. et al., 2004, MNRAS, 355, 608
Gebhardt K., 2004, in Ho L.C., ed., Coevolution of Black Holes and Galaxies, Carnegie Observatories Centennial Symposia. Cambridge Univ. Press, Cambridge, p. 248
Gebhardt K., Fischer P., 1995, AJ, 109, 209
Gebhardt K. et al., 1996, AJ, 112, 105
Gebhardt K. et al., 2000, AJ, 119, 1157
Gebhardt K. et al., 2003, ApJ, 583, 92
Gerhard O., 2005, in Stanghellini L., Walsh J. R., Douglas N. G., eds, Planetary Nebulae Beyond the Milky Way, ESO Astrophysics Symposia, preprint (astroph/0502037)
Gerhard O., Kronawitter A., Saglia R. P., Bender R., 2001, AJ, 121, 1936

Gutierrez C. M., Lopez-Corredoira M., 2005, ApJ, 622, 89
Harris W. E., 1996, AJ, 112, 1487
Harris W. E., 2001, in Labhardt L., Binggeli B., eds, Star Clusters, Saas-Fee Advanced Course 28. Springer-Verlag, Berlin
Hernquist L., Bolte M., 1993, in Smith G. H., Brodie J. P., eds, ASP Conf. Ser., Vol. 48, The Globular Cluster–Galaxy Connection. Astron. Soc. Pac., San Francisco, p. 788
Humphrey P. J., Buote D. A., Gastaldello F., Zappacosta L., Bullock J. S., Brighenti F., Mathews W. G. 2006, ApJ, 646, 899
Irwin J. A., Athey A. E., Bregman J. N., 2003, ApJ, 587, 356
Jarrett T. H., Chester T., Cutri R., Schneider S. E., Huchra J. P., 2003, AJ, 125, 525
Kronawitter A., Saglia R. P., Gerhard O., Bender R., 2000, A&AS, 144, 53
Kundu A., Whitmore B. C., 2001, AJ, 121, 2950
Larsen S. S., Brodie J. P., Huchra J. P., Forbes D. A., Grillmair C. J., 2001, AJ, 121, 2974
Lauer T. et al., 2005, AJ, 129, 2138
McLachlan G. J., Basford K. E., 1988, Mixture Models. Inference and Applications to Clustering, Statistics: Textbooks and Monographs. Dekker, New York
Mamon G. A., Lokas E. L., 2005, MNRAS, 363, 705
Marinoni C., Hudson M. J., 2002, ApJ, 569, 101
Mathews W. G., Brighenti F., 2003, ARA&A, 41, 191
Mei S. et al., 2006, ApJ, in press
Napolitano N. R. et al., 2005, MNRAS, 357, 691
O'Sullivan E., Forbes D. A., Ponman T. J., 2001, MNRAS, 328, 461
Peng E. W., Ford H. C., Freeman K. C., 2004a, ApJ, 602, 685
Peng E. W., Ford H. C., Freeman K. C., 2004b, ApJS, 602, 705
Pierce M. et al., 2006a, MNRAS, 366, 1253
Pierce M. et al., 2006b, MNRAS, 368, 325
Pinkney J. et al., 2003, ApJ, 596, 903
Pryor C., Meylan G., 1993, in Djorgovski S. G., Meylan G., eds, ASP Conf. Ser., Vol. 50, The Structure and Dynamics of Globular Clusters. Astron. Soc. Pac., San Francisco
Randall S. W., Sarazin C. L., Irwin J. A., 2004, ApJ, 600, 729
Richtler T. et al., 2004, AJ, 127, 2094
Robin A. C., Reyle C., Derriere S., Picaud S., 2003, A&A, 409, 523
Romanowsky A. J., 2006a, in Stanghellini L., Walsh J. R., Douglas N. G., eds, ESO Workshop: Planetary Nebulae Beyond the Milky Way. Springer-Verlag, Berlin, p. 294
Romanowsky A. J., 2006b, in Mamon G. A., Combes F., Deffayet C., Fort B., eds, EAS Publ. Ser. Vol. 20, Proc. XXIst IAP Colloq., Mass Profiles and Shapes of Cosmological Structures. EDP Sciences, Paris, p. 119
Romanowsky A. J., Douglas N. G., Arnaboldi M., Kuijken K., Merrifield M. R., Napolitano N. R., Capaccioli M., Freeman K. C., 2003, Sci, 301, 1696
Sambhus N., Gerhard O., Mendez R. H., 2006, AJ, 131, 837
Sarazin C. L., Kundu A., Irwin J. A., Sivakoff G. R., Blanton E. L., Randall S. W., 2003, ApJ, 595, 743
Schlegel D., Finkbeiner D., Davis M., 1998, ApJ, 500, 525
Schwarzschild M., 1979, ApJ, 232, 236
Sharples R. M., Zepf S. E., Bridges T. J., Hanes D. A., Carter D., Ashman K. M., Geisler D., 1998, AJ, 115, 2337
Swartz D. A., Ghosh K. K., Tennant A. F., Wu K., 2004, ApJS, 154, 519
Thomas J., Saglia R. P., Bender R., Thomas D., Gebhardt K., Magorrian J., Richstone D., 2004, MNRAS, 353, 391
Thomas J., Saglia R. P., Bender R., Thomas D., Gebhardt K., Magorrian J., Corsini E. M., Wegner G., 2005, MNRAS, 360, 1355
Trager S. C., Faber S. M., Worthey G., Gonzalez J. J., 2000, AJ, 119, 1645
Trinchieri G., Fabbiano G., Kim D.-W., 1997, A&A, 318, 361
van der Marel R. P., 1991, MNRAS, 253, 710
Vitvitska M., Klypin A. A., Kravtsov A. V., Wechsler R. H., Primack J. R., Bullock J. S., 2002, ApJ, 581, 799
Zepf S. E., 2003, in ESO Workshop: Extragalactic Globular Cluster Systems. Garching, Germany, p. 283
Zepf S. E., Beasley M. A., Bridges T. J., Hanes D. A., Sharples R. M., Ashman K. M., Geisler D., 2000, AJ, 120, 2928

This paper has been typeset from a TEX/LATEX file prepared by the author.